AIP | Applied Physics Letters

In-situ characterization of highly reversible phase transformation by synchrotron X-ray Laue microdiffraction

Xian Chen, Nobumichi Tamura, Alastair MacDowell, and Richard D. James

Citation: Applied Physics Letters **108**, 211902 (2016); doi: 10.1063/1.4951001
View online: http://dx.doi.org/10.1063/1.4951001
View Table of Contents: http://scitation.aip.org/content/aip/journal/apl/108/21?ver=pdfcov
Published by the AIP Publishing

In-situ characterization of highly reversible phase transformation by synchrotron X-ray Laue microdiffraction

Xian Chen,[1,2] Nobumichi Tamura,[2] Alastair MacDowell,[2] and Richard D. James[3]
[1]*Department of Mechanical and Aerospace Engineering, Hong Kong University of Science and Technology, Clear Water Bay, Hong Kong*
[2]*Advanced Light Source, Lawrence Berkeley National Laboratory, Berkeley, California 94720, USA*
[3]*Department of Aerospace Engineering and Mechanics, University of Minnesota, Minneapolis, Minnesota 55455, USA*

(Received 7 February 2016; accepted 4 April 2016; published online 23 May 2016)

The alloy $Cu_{25}Au_{30}Zn_{45}$ undergoes a huge first-order phase transformation (6% strain) and shows a high reversibility under thermal cycling and an unusual martensitc microstructure in sharp contrast to its nearby compositions. This alloy was discovered by systematically tuning the composition so that its lattice parameters satisfy the cofactor conditions (i.e., the kinematic conditions of compatibility between phases). It was conjectured that satisfaction of these conditions is responsible for the enhanced reversibility as well as the observed unusual fluid-like microstructure during transformation, but so far, there has been no direct evidence confirming that these observed microstructures are those predicted by the cofactor conditions. To verify this hypothesis, we use synchrotron X-ray Laue microdiffraction to measure the orientations and structural parameters of variants and phases near the austenite/martensite interface. The areas consisting of both austenite and multivariants of martensite are scanned by microLaue diffraction. The cofactor conditions have been examined from the kinematic relation of lattice vectors across the interface. The continuity condition of the interface is precisely verified from the correspondent lattice vectors between two phases. *Published by AIP Publishing*. [http://dx.doi.org/10.1063/1.4951001]

Materials undergoing reversible phase transformations have potential for emerging applications such as medical devices, sensors/actuators, rechargeable batteries, informative storage, and energy conversion devices.[1–4] Due to the structural change at phase transformation, the mismatch of lattices across the interface leads to the formation of an elastic transition layer between austenite and twinned martensite phases (e.g., the $\beta_1 \rightarrow \gamma_1'$ transformation of CuAlNi[5]). This has been considered as the origin for materials accumulating the thermal hysteresis and losing the reversibility of the transformation upon cycles.[6–9] Satisfaction of the Cofactor Conditions (CC)[5,10] implies that such a transition layer can be eliminated in both single and twinned configurations of austenite and martensite interface microstructure, which has been considered as an effective strategy for lowering the thermal hysteresis, increasing the transformational fatigue resistance, and enhancing the phase reversibility in both the copper-based[11] and nickel-titanium[12–15] based shape memory alloys.

In a typical symmetry-lowering transformation having type I and type II twins consistent with the formal geometry of twinning elements defined by Christian,[16] CC consist of the two conditions:[10] (CC1) the middle principle stretch of transformation stretch tensor is 1, i.e., $\lambda_2 = 1$; (CC2) the length of a 2-fold axis of austenite is preserved for the forward transformation in the case of type II twin, and for the reverse transformation in the case of type I twin. In the case of compound twins that both twinning plane and shearing direction are rational,[17] CC yields different conditions relating to specific twinning parameters (see Chen *et al.*[10]). A necessary consequence of CC is that, theoretically, there exist infinitely many elastically compatible configurations between austenite and multiple martensite variants. That is, no elastic energy will be paid at interfaces during the phase transformation even for highly twinned martensite. By energy minimization, the relationship between (CC1) and energy barrier has been calculated.[13] The minimum hysteresis is reached as $\lambda_2 \rightarrow 1$, which has been experimentally justified in many shape memory alloys.[10,12–14,18] The associated microstructures observed by TEM[19] show the trend that highly twinned martensite becomes twinless as the value of λ_2 approaching 1. Beyond (CC1), two recent discoveries in ZnAuCu[11] and NiTiCu[15] systems show that when both (CC1) and (CC2) are simultaneously satisfied for both type I and type II by special lattice parameters, the functionality will not degrade for million cycles. These results strongly suggest that the (CC2) is responsible for enhancing the phase reversibility, but how it influences the macroscopic deformation through various microstructures is still unclear. In this paper, we will establish an approach to identify the formation of martensite variant *in-situ*, quantify the (CC2), and derive the deformation for phase transformation based on the crystallographic information measured in experiments. $Cu_{25}Au_{30}Zn_{45}$, as the first shape memory alloy satisfies both (CC1) and (CC2) simultaneously, is chosen for this study.

Optical micrographs of $Cu_{25}Au_{30}Zn_{45}$ show a plethora of unusual austenite/martensite interfaces: stripes, curved riverines, zig-zags, and laminae.[11] Furthermore, a great variety of scales has been seen with the optical microscope during consecutive transformation cycles. However, direct quantitative verification between these unusual microstructures and those predicted by CC has not been investigated due to three difficulties: (1) owing to a $\sim 2^\circ$ hysteresis in this alloy, the interface moves quickly out of the field-of-view for scanning-based structural characterization probes; (2) the

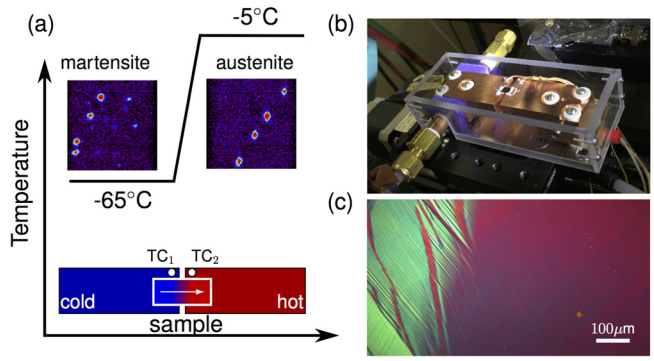

FIG. 1. Experimental setup for *in-situ* microstructural characterization by μSXRD. (a) Schematic experimental arrangement of sample bridging hot and cold copper blocks (lower). Laue patterns of martensite/austenite at −65 °C and −5 °C, respectively (upper). (b) The temperature gradient stage in plexiglass enclosure with top kapton x-ray window removed. (c) The optical micrograph of the phase-transforming interface of $Cu_{25}Au_{30}Zn_{45}$ polished in austenite. (Reprinted with permission from Song *et al.*, Nature **502**(7469), 85–88 (2013). Copyright 2013 Nature Publishing Group.)

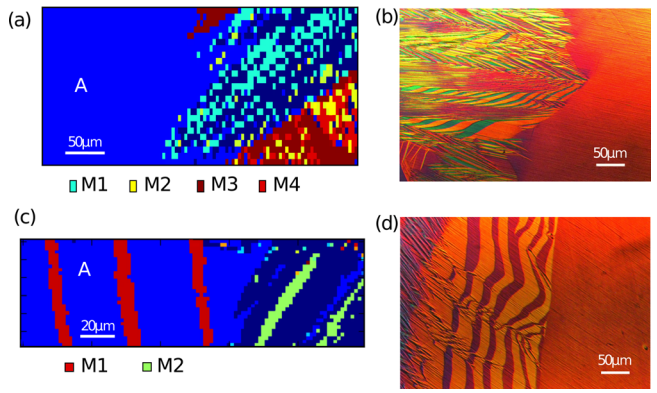

FIG. 2. (a) and (c) Microtopographical configuration in two different transformations from the synchrotron microLaue scan in area of $400 \times 200\,\mu m^2$ and $200 \times 60\,\mu m^2$, respectively. The pixel sizes are $4 \times 10\,\mu m^2$ in (a) and $2 \times 2\,\mu m^2$ in (c). The austenite is denoted by blue, while each of martensite variants is denoted by different color pixels. The dark blue shows the regions that could not be indexed. (b) and (d) The optical micrographs of the same sample in different transformation cycles.

transformation temperature of −40 °C is problematic for instruments sensitive to thermal fluctuations; (3) the low symmetry monoclinic martensite with 72 atoms per unit cell with a long modulated c-axis makes the determination of crystal orientation difficult, especially for electron diffraction methods such as electron backscattering diffraction and high resolution electron transmission microscopy.

For the above reasons, synchrotron X-ray Laue microdiffraction (μSXRD) is a suitable method. This method can characterize the spatial distribution of crystal orientations and deliver the structural parameters using focused polychromatic and monochromatic x-ray beams, respectively. In this letter, we use the state-of-art μSXRD facility at beamline 12.3.2 of the Advanced Light Source, Lawrence Berkeley National Laboratory, to study quantitatively the morphologies of austenite/martensite interfaces in $Cu_{25}Au_{30}Zn_{45}$ undergoing highly reversible martensitic transformation. The X-ray beam with energy bandpass from 6 keV to 22 keV is focused down to 1 μm size by a pair of elliptically bent Kirkpatrick-Baez mirrors. In addition to polychromatic beam (i.e., Laue microdiffraction mode), four bounce monochromatic mirrors are inserted to perform energy scans at the same location probed by the polychromatic beam,[20] which allows sufficient spatial resolution for determination of twins and solve for the complex lattice with high anisotropic unit cell simultaneously.[21] The two-dimensional PILATUS 1M array detector with a high count rate ($>2 \times 10^6$ photons/s) is used for fast Laue pattern collection in areas consisting of both phases. Since the μSXRD probe is insensitive to thermal fluctuations, we can design a proper thermal stage that drives the phase transformation at a low temperature and controls the evolution of the austenite/martensite interface by an external directional temperature gradient.

The design of the thermal stage was implemented using two copper blocks separated by a small gap bridged by a thin slice of sample shown schematically in Figure 1(a). A suitable temperature gradient across the sample is created by passively cooling one copper block with the cryo-nitrogen gas while actively heating the other copper block with an electrical resistance heater. The whole stage is enclosed in a plexiglass box with the top covered by the kapton tape that acts as a window allowing the sample illuminated by x-rays and subsequent transmission of the diffracted x-rays. The stage enclosure is filled with dry nitrogen gas to reduce thermal convection and avoid the formation of frost at low temperature (see Figure 1(b)). The copper blocks are thermally insulated by ceramic standoffs mounted from a kinematic mounting part adapted to the beamline 12.3.2 scanning stage. Two thermocouples, TC_1 and TC_2 in Figure 1(a), record the block temperatures near the gap. TC_2 is also used as a feedback for the heater to stabilize the temperature of the hot copper block. The cryo-stream is generated by passing

TABLE I. Results of the micro LaueScans. **e** is the 2-fold axis of austenite and $\hat{\mathbf{e}} = \mathbf{e}/|\mathbf{e}|$, $X_I = |\mathbf{U}^{-1}\hat{\mathbf{e}}| - 1$, and $X_{II} = |\mathbf{U}\hat{\mathbf{e}}| - 1$.

	Region	Orientation matrix			$\lvert\mathbf{e}\rvert$(Å)	$X_I(10^{-3})$	$X_{II}(10^{-3})$
1	A	0.609	0.032	−0.091	6.1606		
		−0.020	0.610	0.082	8.7124		
		0.094	−0.078	0.604	8.7124		
	M1	−0.365	0.065	−2.474	6.17024	1.459	1.563
		0.068	0.57	−0.065	8.70900	8.020	0.371
		0.247	−0.061	−3.231	8.70914	8.044	0.395
	M2	−0.078	0.564	−0.490	6.17018	1.451	1.555
		−0.258	−0.007	3.184	8.70907	8.029	0.381
		0.355	0.12	2.487	8.70900	8.046	0.397
	M3	0.305	0.049	3.100	6.17020	1.453	1.558
		−0.317	−0.086	2.634	8.70904	8.032	0.384
		0.074	−0.568	−0.131	8.70908	8.033	0.385
	M4	−0.337	−0.050	−2.804	6.17020	1.454	1.558
		−0.291	0.075	2.882	8.70900	8.037	0.389
		0.009	0.57	−0.628	8.70902	8.039	0.39
2	A	0.599	0.132	−0.062	6.1606		
		−0.140	0.594	−0.086	8.7124		
		0.041	0.098	0.607	8.7123		
	M1	−0.250	0.023	−3.490	6.17018	1.457	1.561
		0.367	0.081	−2.048	8.70903	8.026	0.378
		0.042	−0.571	−0.433	8.70900	8.039	0.391
	M2	0.278	−0.158	3.118	6.17019	1.461	1.565
		−0.132	−0.548	−0.486	8.70905	8.025	0.376
		0.323	−0.089	−2.570	8.70906	8.033	0.384

nitrogen gas through a coil in a liquid nitrogen dewar, and the cooling power is controlled by a flow meter. The austenite/martensite interface is trapped at the gap and its position controlled by a steep linear temperature gradient established by powering up the electrical heater and running the cryostream with a constant rate of 7.86 cm^3/s. The actual morphology of the transition varied widely as observed in Song *et al.*,[11] and a typical example is shown in Figure 1(c).

A thin slice $Cu_{25}Au_{30}Zn_{45}$ with dimensions 5 mm × 5 mm × 0.5 mm transforms reversibly between cubic and monoclinic at −40 °C with about 2 °C thermal hysteresis. The sample was polished at room temperature (in austenite) and mounted to the stage shown in Figure 1(c). After temperatures in TC_1 and TC_2 were stabilized around −65 °C and −5 °C, respectively, we start a microLaue line scan across the gap between the two blocks. The Laue pattern at each position on the sample surface is used to identify the phase and orientation of unit cell of the lattice because the number and the symmetry of diffractions are different among the cubic austenite and different variants of monoclinic martensite. The austenite/martensite interface can be detected by locating the scanned position where the symmetry of the Laue patterns switches. Figure 1(a) shows the Laue patterns collected near the austenite/martensite interface where the symmetry of diffraction spots changes from one crystal structure to the other.

To examine diverse interface morphologies of $Cu_{25}Au_{30}Zn_{45}$, we did two microLaue scans for different transformation cycles: LaueScan 1 with step: 4 μm × 10 μm and

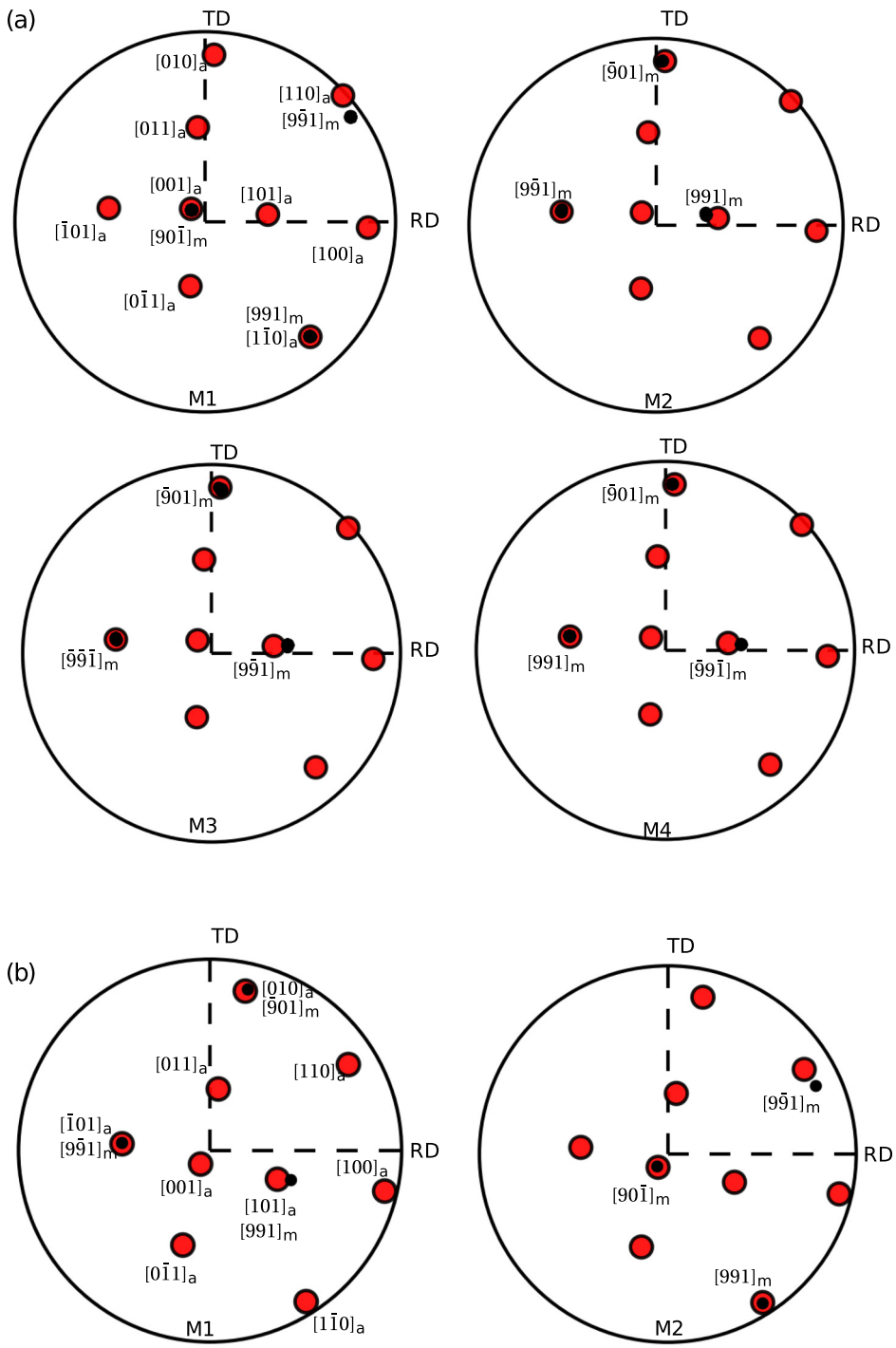

FIG. 3. Stereographic projections of the spatial orientation relationships between austenite 2-fold axes (red dots) and the corresponding martensite lattice vectors (black dots) for (a) LaueScan 1: subregions M1, M2, M3, and M4; (b) LaueScan 2: subregions M1 and M2. TD and RD are the transverse direction and rolling direction of the stage, respectively.

LaueScan 2 with step: $2\,\mu m \times 2\,\mu m$. Holding the conditions constant, the same sample was imaged under the optical microscope for comparison, as shown in Figures 2(b) and 2(d). The irregular zig-zag and single stripe morphologies are seen in both microtopographs generated by microLaue scans and optical microscopy. Since the images in Figures 2(a)–2(d) are captured in different transformation cycles, the interface configurations among them are not exactly the same.

We use the space group $Fm\bar{3}m$ for austenite with 4 Au sites: $4a$ at $(0,0,0)$, 4 Cu sites: $4a$ at $(0,1/2,1/2)$, and 8 Zn sites: $4b$ at $(1/2,1/2,1/2)$, and the space group $P2_1$ for martensite with 18 Au sites: $2a$ at $(3/4,0,z_1+n/9)$, 18 Cu sites: $2a$ at $(1/4,0,z_2+n/9)$, and 36 Zn sites: $2a$ at $(3/4, 1/4, z_2+n/9)+2a$ at $(1/4,1/4,z_1+n/9)$ $(n=1,2,\ldots,9)$ to index the Laue pattern and to get the orientation matrices for austenite and martensite, respectively.[20] The spatial orientations from a microLaue scan consisting of thousands of Laue patterns are analyzed and calculated by the parallel version of the XMAS code on the Carver cluster at the National Energy Research Scientific Computing Center (NERSC). Figures 2(a) and 2(c) show the microtopographs for LaueScan 1 and 2, respectively, in which various colors represent different spatial orientations whereas the dark blue corresponds to the regions neither indexed by austenite nor martensite. The orientation matrices for each of the regions are listed in Table I. For the indexed (hkl) planes, we precisely measured their interplanar distances by a monochromatic energy scan[22] and refined the lattice parameters to be $a_0=6.16061$ Å (austenite), and $a=4.45879$ Å, $b=5.76844$ Å, $c=40.6984$ Å, $\beta=86.79^\circ$ (martensite). Using the *StrucTrans* algorithm,[23] the transformation stretch tensor for such a phase transformation can be calculated and the first condition of CC can be quantified precisely, i.e., in LaueScan 1, $\lambda_2(M1)=1.00061475$, $\lambda_2(M2)=1.00060662$, $\lambda_2(M3)=1.00060613$, and $\lambda_2(M4)=1.00060756$ and in LaueScan 2, $\lambda_2(M1)=1.00061044$ and $\lambda_2(M2)=1.00061361$.

The second condition of CC requires the examination of length change along certain 2-fold axis of austenite. For the austenite with $Fm\bar{3}m$ symmetry, the possible 2-fold axes are three of $\langle 100\rangle_a$ and six of $\langle 110\rangle_a$. They are directly plotted in stereographs in Figure 3 with respective to the Rolling Direction, Transverse Direction, and Normal Direction of the stage for LaueScan 1 and 2, respectively. The red dots in all stereographs denote the 2-fold axes of austenite, while the black dots are the $\langle 901\rangle_m$ and $\langle 991\rangle_m$ directions of the corresponding martensite variant. Table I compares the length between the 2-fold axis in austenite and its corresponding direction in martensite. The $\langle 100\rangle_a$ axis undergoes 0.15% average extension, and the $\langle 110\rangle_a$ axis undergoes 0.038% average compression.

From the orientation relationships indicated in Figure 3, we can calculate the deformation gradient $\mathbf{F}=\sum_{i=1}^{3}\mathbf{g}_i\otimes\mathbf{f}^i$, where $\mathbf{f}^i$ is the set of reciprocal lattice vectors of austenite such that the real lattice vectors $\mathbf{f}_i$ correspond to the lattice vectors of martensite $\mathbf{g}_i$ during the phase transformation. Take the M1 region in LaueScan 2 as an example, $\mathbf{f}_1=\mathbf{O}_a[010]_a$, $\mathbf{f}_2=\mathbf{O}_a[\bar{1}01]_a$, and $\mathbf{f}_3=\mathbf{O}_a[101]_a$ correspond to $\mathbf{g}_1=\frac{1}{9}\mathbf{O}_{m1}[\bar{9}01]_m$, $\mathbf{g}_2=\frac{1}{9}\mathbf{O}_{m1}[9\bar{9}1]_m$, and $\mathbf{g}_3=\frac{1}{9}\mathbf{O}_{m1}[991]_m$. Using the orientation matrices, $\mathbf{O}_{a,m1}$ are directly measured by μSXRD, which is also listed in Table I, the deformation gradient of M1 region in LaueScan 2 can be calculated as

$$\mathbf{F}=\begin{bmatrix}1.0572 & 0.0049 & -0.0554\\ 0.0092 & 1.0015 & -0.0119\\ 0.0627 & 0.0130 & 0.9346\end{bmatrix}. \quad (1)$$

The difference between $\mathbf{F}$ and $\mathbf{I}$ is close to a rank-1 matrix, i.e., the Frobenius norm $||\mathrm{cof}(\mathbf{F}-\mathbf{I})||=0.00075$, where "cof" denotes the cofactor of a matrix. According to the geometrically nonlinear theory of elasticity, the rank-1 connection between two deformation gradients is the necessary and sufficient condition for the existence of an undistorted interface,[24] which implies that the region M1 is compatible with the austenite without elastic transition layer. The interface normal can be solved from the crystallography equations of martensite for variant M1, i.e., $\mathbf{m}=(0.0854,\ 0.0131,\ -0.0864)$ written in the cubic base of austenite. The examination of rank-1 connection from the measurement of μSXRD enlightens a way to show the coherency of interface between two crystal structures at continuum scale. The same calculation can be done using the orientation matrices in Table I for other martensite variants.

The deformation gradient $\mathbf{F}$ in Equation (1) can be used to model the deformed configuration of the region M1 measured in Figure 2(b). In 3D, the interface grows into the sample with an angle from the surface (Figures 4(d) and 4(e)). The projection of the interface can be calculated as $\mathbf{m}-(\mathbf{m}\cdot\mathbf{N}_3)\mathbf{N}_3$, where $\mathbf{N}_3$ is the Normal Direction written

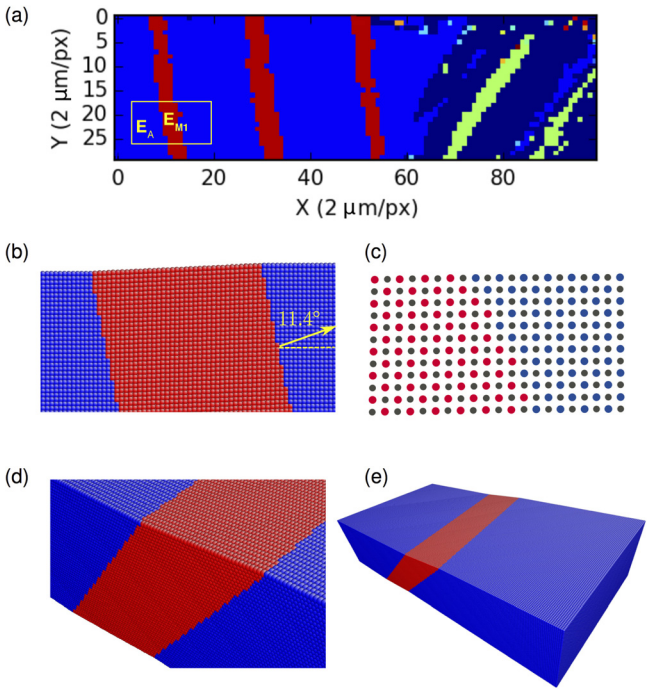

FIG. 4. Macroscopic deformation and lattice distortion of a single variant of martensite calculated from the orientation matrices of $\mathbf{E}_A$ and $\mathbf{E}_{M1}$: (a) austenite/martensite interface morphology mapped directly from microLaue scan II; (b) homogenous deformation of martensite single variant (red) and the stress-free interface at continuum scale; (c) lattices of austenite and martensite across the interface; (d) and (e) morphology of the interface modeled from the deformation gradient in three-dimensions.

in the cubic base of austenite. The angle between the projected interface normal and the rolling direction is 11.4°, which agrees well with the microLaue measurement shown in Figure 4(a). In Figure 4(c), we use the deformation gradient **F** in Equation (1) to generate a homogenous deformation **Fx** for all austenite lattice vectors $\mathbf{x} \cdot \mathbf{m} < 0$, i.e., the red lattice, and leave the rest lattice vectors $\mathbf{x} \cdot \mathbf{m} \geq 0$ undeformed, i.e., the blue lattice. The lattice points between the deformed and undeformed lattices match perfectly without any atomic scale distortions. This shows that the transition layer between the two lattices is eliminated at an atomistic scale due to the satisfaction of compatibility conditions at a continuum scale.

In summary, from the *in-situ* measurement of the orientation matrices for both austenite and martensite across the interface by the synchrotron x-ray Laue microdiffraction, together with the theoretical calculation of the homogenous deformations, we have verified, directly and quantitatively, that the satisfaction of the conditions of compatibility with lattice parameters results in the elastically compatible interface, which ultimately lead to the ultra-low fatigue property of phase transformation in martensitic materials. The approach can be generalized to characterize the evolution of microstructure when the transport properties are sensitive to the structural compatibility at the heterogenous phase boundaries.

X.C. and R.D.J. acknowledge the financial support of MURI Project No. FA9550-12-1-0458 (administered by AFOSR). This research is also benefited from the support of XC's Start-up Fund B002-0172-R9358 (by UGC) and from the support of AFOSR (FA9550-15-1-0207), ONR (N00014-14-0714), and NSF/PIRE (OISE-0967140) to R.D.J. The Advanced Light Source is supported by the Director, Office of Science, Office of Basic Energy Sciences, of the U.S. Department of Energy under Contract No. DE-AC02-05CH11231. The data analysis used resources of the National Energy Research Scientific Computing Center, a DOE Office of Science User Facility supported by the Office of Science of the U.S. Department of Energy under Contract No. DE-AC02-05CH11231.

[1]N. B. Morgan, "Medical shape memory alloy applications—the market and its products," Mater. Sci. Eng., A **378**(1–2), 16–23 (2004).
[2]N. Meethong, H.-Y. S. Huang, S. A. Speakman, W. C. Carter, and Y.-M. Chiang, "Strain accommodation during phase transformations in Olivine-based cathodes as a materials selection criterion for high-power rechargeable batteries," Adv. Funct. Mater. **17**(7), 1115–1123 (2007).
[3]V. Srivastava, Y. Song, K. Bhatti, and R. D. James, "The direct conversion of heat to electricity using multiferroic alloys," Adv. Energy Mater. **1**(1), 97–104 (2011).
[4]J. Liu, T. Gottschall, K. P. Skokov, J. D. Moore, and O. Gutfleisch, "Giant magnetocaloric effect driven by structural transitions," Nat. Mater. **11**(7), 620–626 (2012).
[5]R. D. James and Z. Zhang, "A way to search for multiferroic materials with "unlikely" combinations of physical properties," in *Magnetism and Structure in Functional Materials*, edited by A. Planes, L. Mañosa, and A. Saxena (Springer, Berlin/Heidelberg, 2005), pp. 159–175.
[6]S. Miyazaki, S. Kimura, K. Otsuka, and Y. Suzuki, "The habit plane and transformation strains associated with the martensitic transformation in Ti-Ni single crystals," Scr. Metall. **18**, 883 (1984).
[7]K. Okamoto, S. Ichinose, K. Morii, K. Otsuka, and K. Shimizu, "Crystallography of $\beta_1 \rightarrow \gamma_1'$ stress-induced martensitic transformation in a CuAlNi alloy," Acta Metall. **34**(10), 2065 (1986).
[8]S. Miyazaki, H. Y. Kim, and H. Hosoda, "Development and characterization of Ni-free Ti-based shape memory and superelastic alloys," Mater. Sci. Eng., A **438**, 18 (2006).
[9]A. P. Stebner, S. C. Vogel, R. D. Noebe, T. A. Sisneros, B. Clausen, D. W. Brown, A. Garg, and L. C. Brinson, "Micromechanical quantification of elastic, twinning, and slip strain partitioning exhibited by polycrystalline, monoclinic nickel-titanium during large uniaxial deformations measured via in-situ neutron diffraction," J. Mech. Phys. Solids **61**, 2302 (2013).
[10]X. Chen, V. Srivastava, V. Dabade, and R. D. James, "Study of the *cofactor conditions*: Conditions of supercompatibility between phases," J. Mech. Phys. Solids **61**(12), 2566–2587 (2013).
[11]Y. Song, X. Chen, V. Dabade, T. W. Shield, and R. D. James, "Enhanced reversibility and unusual microstructure of a phase-transforming material," Nature **502**(7469), 85–88 (2013).
[12]J. Cui, Y. S. Chu, O. O. Famodu, Y. Furuya, J. Hattrick-Simpers, R. D. James, A. Ludwig, S. Thienhaus, M. Wuttig, Z. Zhang, and I. Takeuchi, "Combinatorial search of thermoelastic shape-memory alloys with extremely small hysteresis width," Nat. Mater. **5**(4), 286–290 (2006).
[13]Z. Zhang, R. D. James, and S. Müller, "Energy barriers and hysteresis in martensitic phase transformations," Acta Mater. **57**(15), 4332–4352 (2009).
[14]R. Zarnetta, R. Takahashi, M. L. Young, A. Savan, Y. Furuya, S. Thienhaus, B. Maaß, M. Rahim, J. Frenzel, H. Brunken, Y. S. Chu, V. Srivastava, R. D. James, I. Takeuchi, G. Eggeler, and A. Ludwig, "Identification of quaternary shape memory alloys with near-zero thermal hysteresis and unprecedented functional stability," Adv. Funct. Mater. **20**(12), 1917–1923 (2010).
[15]C. Chluba, W. Ge, R. Lima de Miranda, J. Strobel, L. Kienle, E. Quandt, and M. Wuttig, "Ultralow-fatigue shape memory alloy films," Science **348**(6238), 1004 (2015).
[16]J. W. Christian, *The Theory of Transformations in Metals and Alloys (Part I + II)* (Pergamon, 2002).
[17]K. Bhattacharya, *Microstructure of Martensite: Why It Forms and How It Gives Rise to the Shape-Memory Effect*, Oxford Series on Materials Modeling (Oxford University Press, 2003).
[18]V. Srivastava, X. Chen, and R. D. James, "Hysteresis and unusual magnetic properties in the singular heusler alloy $Ni_{45}Co_5Mn_{40}Sn_{10}$," Appl. Phys. Lett. **97**(1), 014101 (2010).
[19]R. Delville, S. Kasinathan, Z. Zhang, J. V. Humbeeck, R. D. James, and D. Schryvers, "Transmission electron microscopy study of phase compatibility in low hysteresis shape memory alloys," Philos. Mag. **90**(1–4), 177–195 (2010).
[20]N. Tamura, *XMAS: A Versatile Tool for Analyzing Synchrotron X-ray Microdiffraction Data* (Imperial College Press, London, 2014).
[21]K. Moffat, D. Szebenyi, and D. Bilderback, "X-ray laue diffraction from protein crystals," Science **223**(4643), 1423 (1984).
[22]M. Kunz, N. Tamura, K. Chen, A. A. MacDowell, R. Celestre, M. Church, S. Fakra, E. Domning, J. Glossinger, J. Kirschman, G. Morrison, D. Plate, B. Smith, T. Warwick, V. Yashchuk, H. Padmore, and E. Ustundag, "A dedicated superbend x-ray microdiffraction beamline for materials-, geo- and environmental sciences at the Advanced Light Source," Rev. Sci. Instrum. **80**(3), 035108 (2009).
[23]X. Chen, Y. Song, N. Tamura, and R. D. James, "Determination of the stretch tensor for structural transformations," J. Mech. Phys. Solids (published online).
[24]J. M. Ball and R. D. James, "Fine phase mixtures as minimizers of energy," Arch. Ration. Mech. Anal. **100**(1), 13–52 (1987).